Rietveld Texture Analysis of Alumina Ceramics by Neutron Diffraction

Emmanuel Guilmeau,[†] Daniel Chateigner,*[,‡] Tohru S. Suzuki,[§] Yoshio Sakka,*[,§] Catherine Henrist,[∥] and Bachir Ouladdiaf[⊥]

National Institute of Advanced Industrial Science and Technology, Midorigaoka, Ikeda, Osaka 563-8577, Japan, CRISMAT-ENSICAEN Laboratory, UMR CNRS 6508, 6 Bd. Maréchal Juin, 14050 Caen Cedex, France, National Institute for Materials Science, Sengen 1-2-1, Tsukuba, Ibaragi 305-0047, Japan, Center for Applied Technology in Microscopy, University of Liège, Building B6, Sart-Tilman, B4000 Liège, Belgium, and ILL, BP 156, 38042 Grenoble, France

Received June 14, 2004. Revised Manuscript Received October 11, 2004

The orientation distributions of α-Al_2O_3 textured ceramics are determined from neutron diffraction spectra. A curved position-sensitive detector coupled to a tilt angle (χ) scan allowed the whole diffraction pattern treatment in the combined Rietveld−WIMV−Popa algorithm. Four textured alumina ceramics were prepared by slip-casting under a high magnetic field and sintered at 800, 1300, 1400, and 1600 °C. The calculation of the distribution density, correlated to the representation of the normal and inverse pole figures, highlights the influence of the magnetic field and sintering temperature on the texture development. The principal pole figures show a pronounced (00*l*) texture: (001) pole parallel to the direction of slip-casting, and (110) pole with higher distribution density for the directions perpendicular to the expected fiber axis. The inverse pole figures calculated for the fiber direction show a major (001) component for all the samples. With the increasing sintering temperature, the texture strength is enhanced and the *c*-axis distribution is sharper. The effectiveness of the approach for determining the crystallite size is also evident. As a global trend, the calculated crystallite size and observed grain size are similar and increase with the increasing sintering temperature. The mechanism of the texture development in the sintered specimens is certainly initiated from the preferred orientation of the green body after slip-casting under a high magnetic field. The basal texture is enhanced during sintering by selective anisotropic grain growth. We evidenced here the powerfulness of the Rietveld texture analysis to provide a basis for the correlation of texture, microstructural parameters, and anisotropic properties.

Introduction

Texture analysis is being increasingly recognized as an important tool in the characterization of polycrystalline materials in order to understand their anisotropic properties. The texture analysis correlates with the physical properties, texture types and strengths, and microstructural aspects, establishes a physical understanding, and helps in the optimal design of textured materials. The development of texture in α-Al_2O_3 ceramics is required to improve their anisotropic thermal conductivity, optical, electrical, and mechanical properties.[1−3] Due to the anisotropic grain growth, related to the rhombohedral crystal structure of α-Al_2O_3 (Table 1) with close-packed oxygen planes perpendicular to the *c*-axis, numerous suitable process methods, such as hot-forging,[4−8] slip-casting,[9] tape-casting,[10,11,3] template grain growth (TGG),[1,2,12,13] or electrophoretic deposition in a strong

Table 1. Details of α-Al_2O_3 Structural Parameters (Relative (006) and (113) Diffracted Intensities from X-ray and Neutron Source)

formula	Al_2O_3
space group	*R*$\bar{3}$*c*
symmetry	rhombohedral
a (Å)	4.7605 (5)
c (Å)	12.9956 (2)
Al: *z*	0.35216 (3)
Al: *B* (Å^2)	0.5
O: *x*	0.30668 (16)
O: *B* (Å^2)	1

relative diffracted intensity (max = 100)

lattice plane	X-ray	neutrons
(006)	0.51	12.2
(113)	100	100

* Corresponding authors: daniel.chateigner@ismra.fr, and SAKKA.Yoshio@nims.go.jp.
[†] National Institute of Advanced Industrial Science and Technology, Osaka.
[‡] CRISMAT-ENSICAEN Laboratory, Caen.
[§] National Institute for Materials Science, Tsukuba.
[∥] Center for Applied Technology in Microscopy, University of Liège.
[⊥] ILL, Grenoble.

(1) Carisey, T.; Levin, I.; Brandon, D. G. *J. Eur. Ceram. Soc.* **1995**, *15*, 283.
(2) Suvaci, E.; Messing, G. L. *J. Am. Ceram. Soc.* **2000**, *83*, 2041.
(3) DiMarcello, F. V.; Key, P. L.; Williams, J. C. *J. Am. Ceram. Soc.* **1972**, *55*, 509.
(4) Heuer, A. H.; Sellers, D. J.; Rhodes, W. H. *J. Am. Ceram. Soc.* **1969**, *52*, 468.
(5) Ma, Y.; Bowman, K. J. *J. Am. Ceram. Soc.* **1991**, *74*, 2941.
(6) Ma, Y.; Lee, F.; Bowman, K. J. *Mater. Sci. Eng. A* **1994**, *175*, 167.
(7) Cannon, R. M.; Rhodes, W. H.; Heuer, A. H. *J. Am. Ceram. Soc.* **1980**, *63*, 46.
(8) Yoshizawa, Y.; Toriyama, M.; Kanzaki, S. *J. Am. Ceram. Soc.* **2001**, *84*, 1392.
(9) Suzuki, T. S.; Sakka, Y.; Kitazawa, K. *Adv. Eng. Mater.* **2001**, *7*, 490.
(10) Raj, P. M.; Cannon, W. R. *J. Am. Ceram. Soc.* **1999**, *82*, 2619.
(11) Böcker, A.; Bunge, H. J.; Huber, J.; Krahn, W.; Ruska, J. *Textures Microstruct.* **1995**, *24*, 167.
(12) Brandon, D.; Chen, D.; Chan, H. *Mater. Sci. Eng. A* **1995**, *195*, 189.

10.1021/cm049054o CCC: $30.25
Published on Web 12/03/2004

magnetic field,[14,15] can produce preferred orientations in bulk materials. According to the processing treatment, different mechanisms have been reported during the last 55 years to explain the texture development, including recrystallization,[4] dislocation slip,[4,5,16] grain boundary sliding,[16,8] and anisotropic grain growth.[2,3,11,17,18] However, correlating changes in the texture with processing parameters is complex. The particular type of texture often found in α-Al_2O_3 oriented materials is an axially symmetric fiber texture (i.e., random in-plane distribution of crystallite *a* and *b* axes), usually produced by a radial symmetry process (uniaxial hot or cold pressing, slip casting) or developed by tape casting/extrusion deformations followed by sintering. This type of texture can be best characterized by the *c*-axis orientation distribution, but this latter, in the case of slightly oriented materials, is difficult to measure using X-rays because of the low structure factors of all the (00*l*) reflections. To overcome this problem, the solution is to calculate the orientation distribution (OD) of the crystallites from several (*hkl*) distributions, i.e., to acquire as many pole figures as possible for the nonparallel (*hkl*) crystallographic planes. Bocker et al.[19] proposed a procedure to calculate, from the X-ray analysis, the orientation distribution function (ODF) and the related (00*l*) distribution from numerous pole figures. The reliability of the results was proven by comparing the maximum pole densities of various lattices planes measured by X-ray and neutron diffraction. In this approach, the basal-plane pole figure can be directly and accurately measured, since the (006) neutron structure factor is much higher than the corresponding X-ray structure factor (relative (001) and (113) diffracted intensities from X-ray and neutron sources are specified in Table 1). Working within the framework that combines the classical Rietveld[20] analysis with texture[21] and grain size[22] analysis, as implemented in the MAUD software[23] (materials analysis using diffraction) or GSAS[24] (general structure analysis system), permits a comprehensive approach to the crystal structure−texture−microstructure analysis. The increasing number of papers based on this methodology illustrates the interest of many researchers in materials science for Rietveld texture analysis.[25−33] Herein, we illustrate the advantages of jointly analyzing the structure

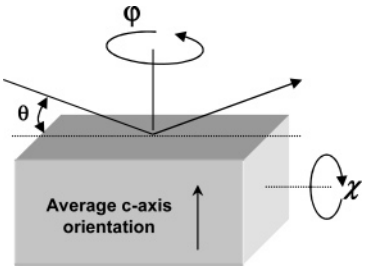

Figure 1. Schematics of the geometry used for the neutron texture analysis.

(Rietveld), texture (WIMV), and microstructure (Popa), of α-Al_2O_3 ceramics. We use the neutron data of textured specimens synthesized with different processing parameters to illustrate the high efficiency and accuracy of the software to extract the texture and mean crystallite sizes. The mechanism of texture development during the sintering treatment is discussed.

Experimental Section

The materials were processed using the slip-casting method.[9,34−36] A high magnetic field of 10 T, parallel to the slip casting direction, was applied to a suspension of fine α-Al_2O_3 spherical particles ($\varnothing \approx 150$ nm) at room temperature. Due to the anisotropic magnetic susceptibility of the rhombohedral structure, the high magnetic field applied during the slip-casting is highly effective in rotating the particles and generating a (001) preferred orientation parallel to the magnetic field.[9] The same phenomena associated with strong magnetic fields have already been reported for high-T_c superconductors[37,38] for which the energy of anisotropy is strong enough to align particles in a magnetic field. The green bodies obtained after filtration were further compacted by cold isostatic pressing (CIP) at 392 MPa for 10 min. Four samples were prepared by sintering at 800, 1300, 1400, and 1600 °C. The specimens were measured using the D1B neutron line at the Institut Laue Langevin, Grenoble, France. The neutron wavelength is monochromatized to $\lambda = 2.523$ Å. Diffracted neutrons are collected by a curved position-sensitive detector composed of 400 cells spread over 80° (resolution 0.2°) in 2θ. A Eulerian cradle allows the χ angle rotation. Scans were operated from $\chi = 0$ to 90° (step 5°) using a fixed incidence angle ω of 35.6° ({006} Bragg position). Since the samples have an axially symmetric (fiber) texture, as expected by the processing radial symmetry and confirmed by azimuthal rotation (φ), the complete texture determination can be obtained by only tilting the sample (χ rotation) with the φ rotation being unnecessary (Figure 1). From the nineteen 2θ scans measured for the different sample

(13) Seabough, M. M.; Kerscht, I. H.; Messing, G. L. *J. Am. Ceram. Soc.* **1997**, *80*, 1181.
(14) Uchikoshi, T.; Suzuki, T. S.; Okuyama, H.; Sakka, Y. *J. Mater. Res.* **2004**, *19*, 1487.
(15) Uchikoshi, T.; Suzuki, T. S.; Okuyama, H.; Sakka, Y. *J. Mater. Sci.* **2004**, *39*, 861.
(16) Heuer, A. H.; Tighe, N. J.; Cannon, R. M. *J. Am. Ceram. Soc.* **1980**, *63*, 53.
(17) Böcker, A.; Bunge, H. J.; Huber, J.; Krahn, W. *J. Eur. Ceram. Soc.* **1994**, *14*, 283.
(18) Seabaugh, M. M.; Messing, G. L. *J. Am. Ceram. Soc.* **2000**, *83*, 3109.
(19) Böcker, A.; Brokmeier, H. G.; Bunge, J. *J. Eur. Ceram. Soc.* **1991**, *8*, 187.
(20) Rietveld, H. M. *J. Appl. Crystallogr.* **1969**, *2*, 65.
(21) Matthies, S.; Vinel, G. W. *Phys. Status Solidi B* **1982**, *112*, 111.
(22) Popa, N. C. *J. Appl. Crystallogr.* **1998**, *31*, 176.
(23) Lutterotti, L.; Matthies, S.; Wenk, H. R. *Proceedings of the 12th International Conference on Textures of Materials*, Vol. 2; Szpunar, J. A., Ed.; NRC Research Press: Montreal, 1999, pp 1599−1604. Freeware available at: http://www.ing.unitn.it/~luttero/maud/.
(24) Von Dreele, R. B. *J. Appl. Crystallogr.* **1997**, *30*, 517.
(25) Guilmeau, E.; Lambert, S.; Chateigner, D.; Noudem, J. G.; Ouladdiaf, B. *Mater. Sci. Eng. B* **2003**, *104*, 107.
(26) Guilmeau, E.; Chateigner, D.; Noudem, J.; Funahashi, R.; Horii, S.; Ouladdiaf, B. *J. Appl. Crystallogr.*, submitted for publication.
(27) Wenk, H. R.; Cont, L.; Xie, Y.; Lutterotti, L.; Ratschbacher, L.; Richardson, J. *J. Appl. Crystallogr.* **2001**, *34*, 442.
(28) Morales, M.; Chateigner, D.; Fruchart, D. *J. Magn. Magn. Mater.* **2003**, *257*, 258.
(29) Morales, M.; Chateigner, D.; Lutterotti, L.; Ricote, J. *Mater. Sci. Forum* **2002**, *408−412*, 113.
(30) Bae, J−H.; Heo, G.; Oh, S. T.; Shin, E.; Seong, B−S.; Lee, C.-H.; Oh, K. H. *Mater. Sci. Forum* **2002**, *408−412*, 215.
(31) Xie, Y.; Wenk, H.-R.; Matthies, S. *Tectonophysics* **2003**, *370*, 269.
(32) Lutterotti, L.; Matthies, S.; Wenk, H.-R.; Schultz, A. S.; Richardson, J. W., Jr. *J. Appl. Phys.* **1997**, *81*, 594.
(33) Wenk, H.-R.; Lutterotti, L.; Vogel, S. *Nucl. Instrum. Methods Phys. Res., Sect. A* **2003**, *515*, 575.
(34) Sakka, Y.; Suzuki, T. S.; Kitazawa, K. *Key Eng. Mater.* **2002**, *206−213*, 349.
(35) Suzuki, T. S.; Sakka, Y. *Jpn. J. Appl. Phys.* **2002**, *41*, L1272.
(36) Suzuki, T. S.; Sakka, Y. *Chem Lett.* **2002**, *12*, 1204.
(37) Beaugnon, E.; Tournier, R. *Nature* **1991**, *349*, 470.
(38) Noudem, J. G.; Beille, J.; Bourgault, D.; Tournier, R. *Physica C* **1996**, *264*, 325.

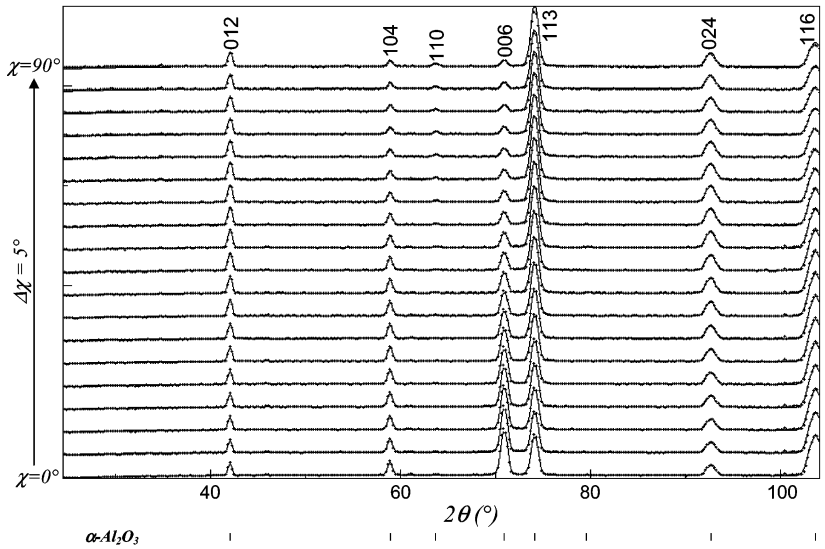

Figure 2. Neutron diffraction patterns obtained for our samples using a 0−90° χ-scan (sample sintered at 1300 °C). Diffracted peaks are indexed. Dotted lines represent measured diffraction intensities, solid lines represent fitted curves.

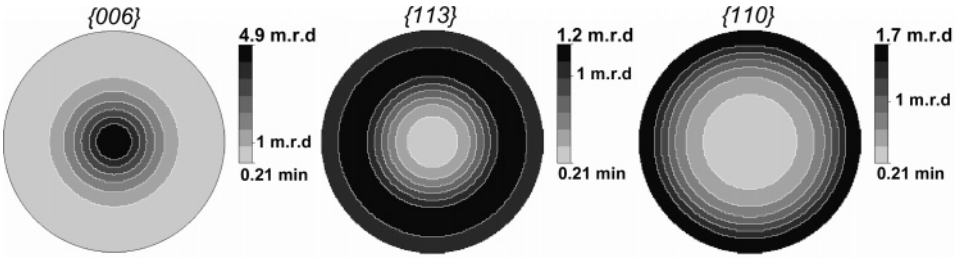

Figure 3. {006}, {113}, and {110} pole figures recalculated from the refined OD. Sample sintered at 1300 °C. Linear density scale, equal area projection.

orientations, each sample was analyzed by the same procedure. First, the integrated intensities were extracted by the Le Bail algorithm,[39] and used for a first refinement of the OD by the WIMV formalism. The OD obtained was then introduced in the cyclic Rietveld refinement. The new refined parameters were used for a new WIMV cycle to correct the OD, and so on. Several cycles of refinement were performed to converge toward a final characterization of the material. The refinement quality was assessed by the comparison of the experimental and recalculated diagrams and by the reliability factors: RP0 and RP1 for the OD refinement,[32] and RB and R_w for the Rietveld refinement.[40] The instrumental profile has been calibrated using a standard calcite specimen (large crystallite sizes and no microstrains). The average volume of our samples is around 350 mm^3, and the measuring time for a single spectrum is 20 min. It is important to note that the neutron diffraction (transmission) has two advantages. First, there is no defocusing effect (occurring in X-ray) and it consequently allows all the peaks to strongly scatter up to $\chi = 90°$. Second, as mentioned above, the calculation of the *c*-axis distribution is easier by neutron diffraction for which the structure factor of the (006) peak is higher than that for X-rays.

Results and Discussion

Figure 2 shows the typical neutron diffraction pattern obtained for our samples using a 0−90° χ-scan (sample sintered at 1300 °C). This graph highlights without ambiguity the (001) texture of the α-alumina. In particular, we can clearly observe the intensity decrease of the (006) line when χ increases and the appearance of the (110) line when χ tends to 90°. We can also visually appreciate the agreement between the experimental (dots) and refined (lines) spectra for all the χ orientations. The refinement reliability is established by RP0, RP1, R_w, and RB factors equal to 4.6%, 4.1%, 6.5%, and 4.8%, respectively.

Figure 3 shows the {006}, {113}, and {110} pole figures recalculated from the refined OD. The {006} pole figure exhibits a strong maximum of c-axes parallel to the sample normal. The {113} pole figure presents a small circle at the χ position around 60°, a value equal to the angle between the (001) and (113) directions in the rhombohedral structure. The maximum of the distribution density around $\chi = 90°$ for the {110} pole figure is also compatible with the expected fiber texture and the structure. From the point of view of the texture development, it is really important to check which (*hkl*) planes align with their normals along the *z* axis (normal to sample surface), which cannot be evidenced directly by only the pole figures in the given 2θ range. For instance, if small textural components with ⟨*hkl*⟩ directions (other than ⟨00*l*⟩) also align with the sample normal, these would not be easily visible on the pole figures of Figure 3 themselves, though they would contain all the information. To visualize these eventual small components, the full representation of the OD is required, which in the case of the fiber textures can be represented by the inverse pole figures (Figure 4) calculated for the *z* fiber direction, parallel to the magnetic field. This figure illustrates two interesting points. First, it shows that the only component present in the four samples is with the (00*l*) crystallographic planes perpendicular to the

(39) Le Bail, A. *Mater. Res. Bull.* **1988**, *23*, 447.
(40) Young, R. A.; Wiles, D. B. *J. Appl. Crystallogr.* **1982**, *15*, 430.

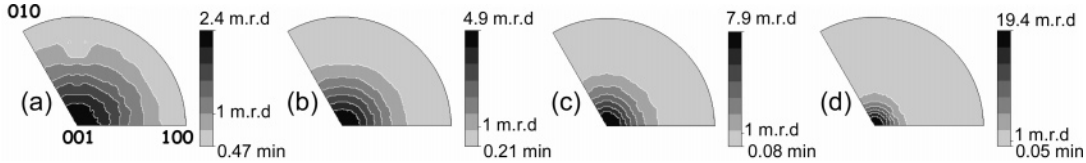

Figure 4. Inverse pole figures calculated for the *z* fiber direction (parallel to the magnetic field) for samples sintered at (a) 800, (b) 1300, (c) 1400, and (d) 1600 °C. Major (001) component. Linear density scale, equal area projection.

Table 2. Minima and Maxima of (001) Inverse Pole Figures and Texture Index[a]

specimens (sintering temp., °C)	ODF (001) inverse pole figure min (m.r.d)	ODF (001) inverse pole figure max (m.r.d)	texture index (F_2) (m.r.d^2)	refined crystallite size (nm)	SEM calculated grain size (nm) $d_{\|}$	SEM calculated grain size (nm) $d_{\perp}$	aspect ratio ($d_{\perp}/d_{\|}$)
800	0.47	2.4	1.24	137 (13)	∼150 (manually)		∼1
1300	0.21	4.9	2.13	> 500 nm	1100	1170	1.063
1400	0.08	7.9	3.16	> 500 nm	2610	2970	1.138
1600	0.05	19.4	7.78	> 500 nm	7300	8800	1.205

[a] Refined crystallite size and grain size determined by line intercept method (SEM), parallel ($d_{\|}$) and perpendicular ($d_{\perp}$) to the magnetic field direction. Spherical grain size of the specimen sintered at 800 °C was determined manually.

slip-casting direction. Second, the degree of orientation is improved for the higher sintering temperatures: the maximum of the distribution density is increased and the *c*-axis distribution gets sharper. Based on the peak deconvolution (Popa formalism), the calculated crystallite sizes have been found to be equal to 140 nm for the sample sintered at 800 °C and larger than 500 nm for samples sintered at 1300, 1400, and 1600 °C (crystallite sizes larger than 500 nm are not measurable under our resolution conditions). These sizes are well correlated to SEM analyses where we determined the grain sizes by the linear intercept method on the surface parallel to the magnetic field. The measurement was performed on this surface in two directions, i.e., parallel and perpendicular to the magnetic field. The values, reported in Table 2, evidenced the nearly spherical shape of the grains in the sample sintered at 800 °C, whereas the grain size and the respective aspect ratio increase with increasing sintering time. As illustrations, Figure 5a and b show typical SEM micrographs of the surface parallel to the magnetic field of the samples sintered at 800 and 1600 °C, respectively. Due to the low relative density (65%) of the sample sintered at 800 °C, the polishing was quite difficult and did not allow the achievement of a clean and flat surface. The grain size has been manually determined in that case and not by the linear intercept method. Finally, to summarize the results, Table 2 offers a comparison between the texture analysis, crystallite size refinement, and grain size calculation. The correlation of the calculated (001) distributions, accessed by the texture index[41] values, crystallite sizes, and microstructural observations, clearly proves that the growth of the initial small spherical particles starts at temperatures above 800 °C, and the enhanced anisotropic grain growth by the increasing sintering temperature is an important factor for the texture development. The analysis appears accurate to extract the small crystallite size and demonstrates the high crystallinity of the grains which have a size comparable to the crystallites. Because of the insuficient neutron experimental resolution, the anisotropic crystallite size of the samples sintered at 1300, 1400, and 1600 °C, using the Popa size algorithm, could not been refined. Further investigations by X-ray analysis will be done to clarify, if possible, this point.

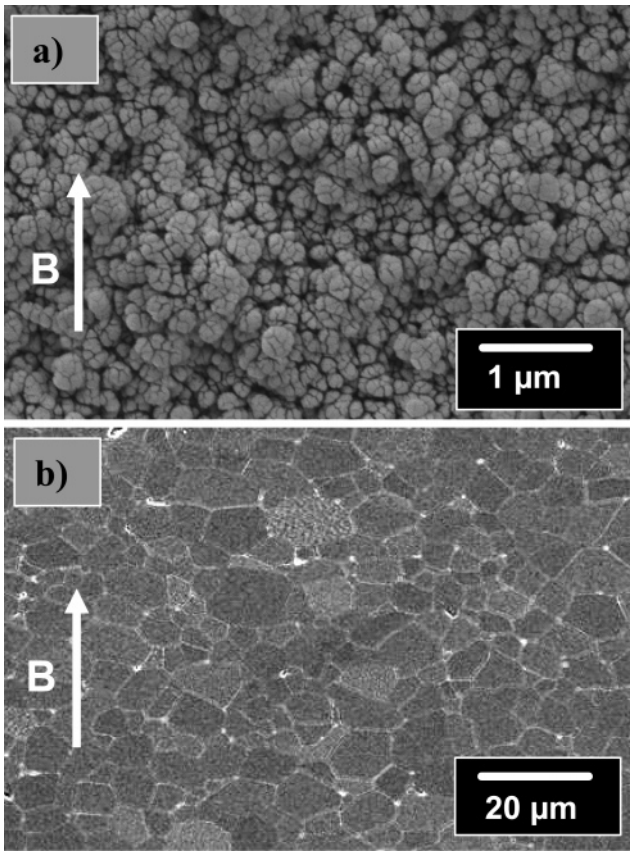

Figure 5. SEM observation of samples sintered at (a) 800 and (b) 1600 °C. The direction of the magnetic field (B) applied parallel to the slip-casting direction is indicated.

A final consideration is the mechanism of formation of the texture observed in these Al_2O_3 ceramics. It is first evidenced from the observation and calculation of the crystallite size that the sample sintered at 800 °C did not engage the grain growth. It is then clear that the origin of the texture in this sample (Figure 4a) is related to the magnetic field applied during the slip-casting process. It must be noted that experiments without applied magnetic field during slip-casting lead to the absence of any significant texture in the body specimen as in the sintered samples.[9]

(41) Bunge, H. J. *Texture Analysis in Materials Science*; Butterworth: London, 1982.

This result is in agreement with the Jeffery's model[42] for which only anisotropic shapes (platelets, needles, etc.) are susceptible to generating preferred orientations during the movement of rigid crystals embedded in a melt. As a consequence, we proved the effectiveness of our technique and the real role of the magnetic field during slip-casting to generate a preferential orientation in the green body. On the other hand, as we reported above, the enhancement of the texture with the increasing sintering temperature would appear with the anisotropic grain growth. The aspect ratio of the grains, calculated from the SEM observations and reported in Table 2, indicates the trend to develop anisotropic growth in the direction perpendicular to the magnetic field. Seabough et al.[18] reported that the primary mechanism for texture development in template grain growth (TGG) specimens was coming from the growth of well-oriented templates, excluding a possible template rearrangement. This phenomenon is difficult to put in parallel with our study since the initial powder of our samples is composed of only small spherical grains without templates. However, we can emphasize that the preferential orientation of the green body tends to favor the texture development during firing. Indeed, if adjacent grains have a similar orientation, grain growth will be enhanced in this orientation because of the low grain boundary energy. Consequently, the initial well-aligned particles will favor the development of the basal texture via a drastic grain growth increase when the sintering temperature is increased. We can consider that the texture driving force here is the reduction of the surface free energy of the system by the preferential growth of the initially well-aligned adjacent particles. This assumption is in good agreement with the conclusions reported by Bocker et al.[17] where the authors showed, as we did, that the strongest influence on the final texture is observed for the highest sintering temperature. They emphasized that this increase in the texture strength may be attributed to grain coarsening due to the initial well-aligned big grains growing at the expense of the small grains during sintering, and consequently, enhancing the final texture strength. Finally, the small particle size of the precursor powder ($\varnothing = 150$ nm) is also an important factor to provide the driving force for grain growth. Bocker et al.[11] clearly showed that small particles are necessary to develop a strong texture. Here, the specimen sintered at 1600 °C exhibits a texture strength almost 8 times higher than that of the sample sintered at 800 °C.

Conclusion

This study demonstrates the efficient and reliable use of the iterative combination of algorithms for structure (Rietveld), microstucture (Popa), and OD calculation (WIMV). The Rietveld texture approach was shown to be highly effective for extracting the texture strength and crystallite size in α-Al_2O_3 ceramics. The mechanism of texture development in the sintered specimens, which cannot be completely elucidated at this time, is probably initiated from the preferred orientation of the green body. The basal texture development is then enhanced during sintering by selective anisotropic grain growth. This Rietveld texture methodology, capable of simultaneously refining texture and crystallite size, is promising for generalizing the characterization of the polycrystalline materials and extending the refinement to the determination of the structure, microstrains,[29,43] and phase proportions.[26,27,44] Finally, it provides a basis for the correlation of texture, microstructural parameters, and anisotropic properties. X-ray analyses are now underway for comparison with the present neutron results.

CM049054O

(42) Jeffery, G. B. *Proc. R. Soc. London, Ser. A* **1922**, *102*, 161.
(43) Ricote, J.; Chateigner, D. *J. Appl. Crystallogr.* **2004**, *37*, 91.
(44) Xie, Y.; Lutterotti, L.; Wenk, H.-R.; Kovacs, F. *J. Mater. Sci.* **2004**, *39*, 3329.